



PAPER

Ionization quenching correction for a 3D scintillator detector exposed to scanning proton beams

Fahed Alsanea^{1,2} , Chinmay Darne¹, Daniel Robertson³ and Sam Beddar^{1,2} ¹ Department of Radiation Physics, The University of Texas MD Anderson Cancer Center, Houston, TX, United States of America² The University of Texas MD Anderson UTHealth Graduate School of Biomedical Sciences, Houston, TX, United States of America³ Department of Radiation Oncology, Mayo Clinic Scottsdale-Phoenix, Scottsdale, AZ, United States of AmericaE-mail: abeddar@mdanderson.org**Keywords:** dosimetry, proton therapy, scintillators, ionization quenching, scintillation detectors**Abstract**

The ionization quenching phenomenon in scintillators must be corrected to obtain accurate dosimetry in particle therapy. The purpose of this study was to develop a methodology for correcting camera projection measurements of a 3D scintillator detector exposed to proton pencil beams. Birks' ionization quenching model and the energy deposition by secondary electrons (EDSE) model were used to correct the light captured by a prototype 3D scintillator detector. The detector was made of a 20 cm × 20 cm × 20 cm tank filled with liquid scintillator, and three cameras. The detector was exposed to four proton-beam energies (84.6, 100.9, 144.9, and 161.6 MeV) at The University of Texas MD Anderson Cancer Center's Proton Therapy Center. The dose and track averaged linear energy transfer (LET) were obtained using validated Monte Carlo (MC) simulations. The corrected light output was compared to the dose calculated by the MC simulation. Optical artefact corrections were used to correct for refraction at the air–scintillator interface, and image perspective. These corrections did not account for the non-orthogonal integration of data off the central axis of the image. Therefore, we compared the light output to an integrated MC dose and LET along the non-orthogonal path. After accounting for the non-orthogonal integration of the data, the corrected light output reduced the dose error at the Bragg peak region from 15% to 3% for low proton-beam energies. Overall, the doses at the Bragg peak region using the Birks' model and EDSE model were less than ±3% and ±7% of the MC dose, respectively. We have improved the application of Birks' model quenching corrections in 3D scintillators by numerically projecting the dose and LET 3D grid to camera projections. This study shows that scintillator projections can be corrected using average LET values at the central axes.

1. Introduction

Dosimetric detectors that use volumetric scintillators are of growing interest because they offer fast, accurate, high-resolution measurements of absorbed dose distribution through optical imaging (Fukushima *et al* 2006, Beddar *et al* 2009, Pönisch *et al* 2009, Archambault *et al* 2012, Hui *et al* 2015, Darne *et al* 2017, Almurayshid *et al* 2017). However, in a scintillator medium exposed to beams of protons, or any ionizing radiation beam, the emitted light response is nonlinear to the incident radiation ionization density (Birks 1964). For protons and heavy charged particles, the ionization density can be quantified as the linear energy transfer (LET), which varies as a function of depth. LET increases rapidly in the region of the Bragg peak, resulting in an under-response by the organic scintillator in this region. This phenomenon is called ionization quenching, and it must be addressed in order to use three-dimensional (3D) volumetric scintillator detectors for dose verification.

Robertson *et al* (2013) demonstrated that the Birks equation (Birks 1964) could be used to correct for ionization quenching in a volumetric liquid scintillator; they found dose agreement within ±3% at the Bragg peak for high-energy beams (144.9, and 161.6 MeV) and ±10% for an 85.6 MeV beam. Similarly, Wang *et al*

(2012) found the difference between the corrected light signal (using the Birks equation) and the calculated dose to be within $\pm 5\%$ in a polystyrene-based scintillating fiber exposed to single-energy passive-scattering proton beams. Almurayshid *et al* (2017) also demonstrated quenching corrections using the Birks equation with a volumetric plastic scintillator and a commercially available camera for a 60 MeV proton beam. They reported a range accuracy of 0.2 mm and a Bragg peak/plateau ratio accuracy of 3%.

The nonlinear response of organic scintillators has been explained by the widely used semiempirical model proposed by Birks. This model relates the nonlinear response to LET. The model was extended by Chou (1952) to relate quenching effects to a second order of LET. However, Birks model failed to explain the scintillation response for low energy photons and electrons (Boivin *et al* 2016). Later, Blanc *et al* (1964) proposed a more general model of scintillation by looking at the kinetics of ionization quenching, one that accounted for the temporal aspect and radial diffusion of energy deposition. A simplified version of Blanc's formula becomes the Birks equation. Christensen and Andersen (2018) demonstrated the use of Blanc's model and its advantages for fiber-coupled scintillators exposed to proton beams. The evidence that the nonlinear response of a scintillator depends not only on LET, but also on the particle type, led to explorations of other properties of the energy-loss process for different particles with the same LET. One such property is the energy deposition by secondary electrons. Michaelian and Menchaca-Rocha (1994, 1995) formalized an analytical model of ion-induced luminescence, which was termed the energy deposition by secondary electrons (EDSE), and showed that regions close to the particle track are the source of the nonlinearity of scintillation.

In this work, we compared the performance of two different ionization quenching models, the Birks equation and the EDSE model, for use with volumetric scintillator detectors. We used a large-volume organic liquid scintillator detector that can image 3d dose distributions of proton beams in real time (Darne *et al* 2016). The prototype 3D scintillator detector is based on a previously studied and characterized volumetric scintillator detector used for verification of proton-beam properties (Beddar *et al* 2009, Pönisch *et al* 2009, Archambault *et al* 2012, Robertson *et al* 2014). We also investigated the effects of optics on the values of dose and LET in each pixel.

2. Methods

2.1. 3D scintillator detector

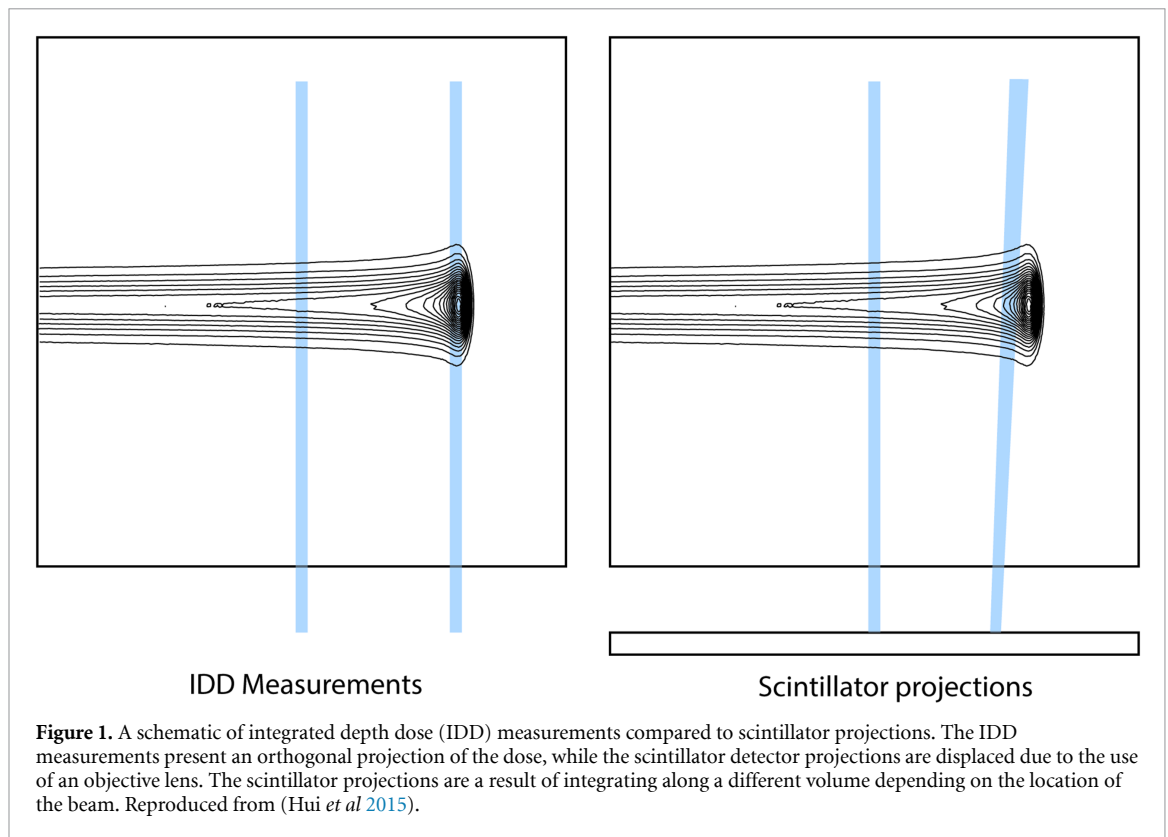
The detector has been characterized in detail by Darne *et al* (2017). The 3D scintillator system consisted of an acrylic tank (20 cm \times 20 cm \times 20 cm) that had three clear sides and three opaque sides and was filled with Optiphase HiSafe 3 liquid scintillator (PerkinElmer, Waltham, MA). To image the light distribution, three Zyla 5.5 scientific complementary metal oxide semiconductor (sCMOS) cameras were used (Andor Technology Ltd., Belfast, UK). The three camera projections view the tank from the front, top, and side. The front and top views are projections x , y , which shows the proton depth dose curve. The side view is projection z , which shows the beams eye view. For this study, we were only interested in projection x (z - y plane), which show the depth-dose distribution (z -direction), for ionization quenching corrections. The cameras were equipped with 20.5 mm fixed-focal-length objective lenses (Schneider Optics, Van Nuys, CA) with an $f/8$ aperture. The cameras were positioned 65 cm from the tank surface. This resulted in a depth of field of 20.5 cm around the center of the tank. The individual pixel size was 6.5 μm and the resulting mean spatial resolution of the system was 0.208 mm.

The sCMOS cameras were operating in the global shutter mode, which captures a frame all at once. The cameras image acquisition were synchronized with the proton beam deliveries (Alsanea *et al* 2019). A background signal was subtracted from the signal images. The camera's SNR was 20 dB at 0.5 cGy (Darne *et al* 2017).

2.2. Irradiation conditions and Monte Carlo simulations

The scintillator detector was exposed to the spot-scanning proton beam at The University of Texas MD Anderson Cancer Center's Proton Therapy Center. This proton-beam system can generate 94 proton-beam energies ranging from 72.5 MeV to 221.8 MeV. For this study, the proton pencil beams were measured and modeled on the basis of the scanning beam nozzle. The energies chosen were 85.6, 100.9, 144.9, and 161.6 MeV. These energies were chosen because they spanned the size of the scintillator tank (20 cm) and were a reasonable subsample of the range of possible energies.

Proton-beam dose distribution and track-averaged LET in 3D were determined using a validated Monte Carlo radiation transport code, MCNPX version 2.7d (Waters *et al* 2002). The phase space models of the scanning beam nozzle at the Proton Therapy Center were validated with dose measurements (Sawakuchi *et al* 2010). The geometry setup of the scintillator detector was reproduced in the Monte Carlo code. The face of the detector was placed at the isocenter at a source-to-surface distance of 270 cm. The voxel size was



$1 \times 1 \text{ mm}^2$ lateral to the beam; in the axial direction, the resolution was 1 mm in the buildup region and 0.1 mm at the Bragg peak. The number of protons simulated was 5×10^7 for each beam energy, resulting in an uncertainty of less than 1% for all voxels with doses exceeding 2% of the maximum dose. All secondary particles were tracked. We scored the energy deposition and particle flux and their uncertainties in each voxel.

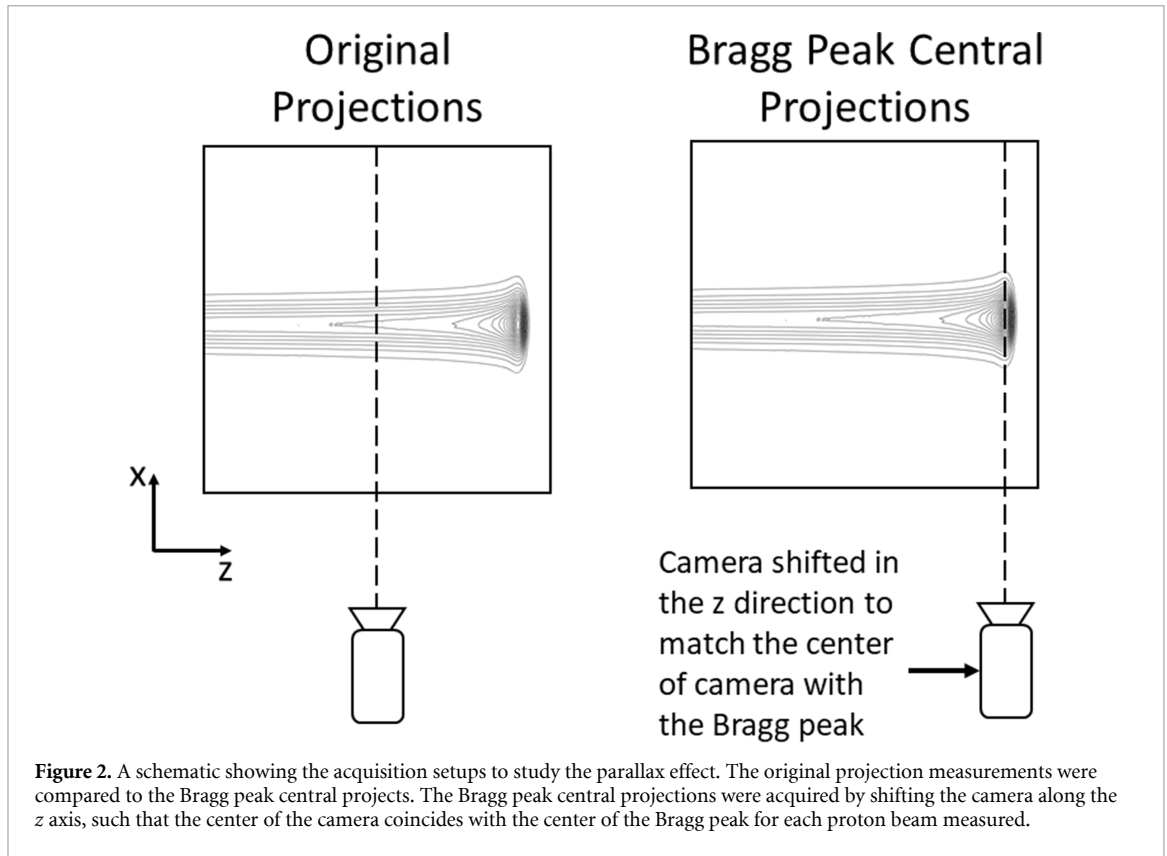
The proton track-averaged LET is defined as the arithmetic mean of the electronic stopping power of all protons in a given region. For clinical proton beam energies, the stopping power can be replaced with track-averaged LET. In this study we used track-averaged LET, which was achieved by dividing the energy deposition in each voxel by the particle fluence. It is possible to use dose-averaged LET in the quenching correction, but its applicability of it in broad LET spectrum at the Bragg peak region is questionable (Grün *et al* 2019, Christensen *et al* 2019). Track-average LET is more appropriate to use for scintillation, because the light yield per unit path length is proportional to the average energy transfer from ionization or excitation per unit length traveled by charged primary particle (Christensen *et al* 2019).

2.3. Image processing: optical simulation

A previously established optical artifact correction and geometric calibration technique was used to correct the acquired images (Robertson *et al* 2014, Hui *et al* 2015). The optical corrections included corrections for refraction at the air–scintillator interface and for image perspective. The lens distortion was corrected using the Camera Calibration Toolbox (Bouquet 2010) for MATLAB (version R2017b; MathWorks, Natick, MA). The geometric calibration determined the optical length from the surface of the tank to the camera sensor, the angular shift, and the translational shift of the tank relative to the camera sensor center.

Parallax errors in camera projections hindered the alignment of the Monte Carlo dose and LET. This is illustrated in figure 1, where the integrated depth-dose profiles are orthogonal to the measurement plane. However, for the scintillator system, the shape and volume of the integrated plane are not orthogonal to the beam axis and differ depending on the location of the measurement. This artifact cannot be corrected for because the projections are already an integrated signal of the light distribution.

Light rays originating away from the tank center will be traveling at an angle from the normal of the front of the camera window. Therefore, we expected that if the Bragg peak were at the center of the system, this artifact would be smaller. To test this, the four proton-beam energies were acquired such that the center of the Bragg peak fell on the center of the camera sensor, as shown in figure 2. This did not completely eliminate the artifact. Therefore, in addition to comparing central and noncentral Bragg peak projections, the simulated 3D dose and average LET distribution were used to obtain a simulated projection that matched the scintillator system using the aforementioned optical properties. A central plane from the 3D distribution was



projected onto a single row of camera pixels to obtain the average LET, and a dose profile was obtained by using a projection matrix that contained refraction and perspective optical artifacts only (i.e. we determined the average LET and dose in the nonorthogonal volume for the scintillator system). The scintillation light was plotted as a function of LET for each beam energy to demonstrate the effect of the parallax error on the assignment of LET values. All image processing and analyses were performed using MATLAB (version R2017b; MathWorks, Natick, MA).

2.4. Quenching correction

In this study, two scintillation models, described in sections 2.4.1 and 2.4.2 below, were used to determine the quenching correction factors. The first model was the semiempirical model developed by Birks (1964). This model is very successful at correcting quenching for a given ion. The second model, the EDSE model (Michaelian and Menchaca-Rocha 1994), has the advantage of being able to correct the response of scintillators exposed to a variety of heavy charged particles with one free parameter. In contrast, the Birks model's quenching parameter has to be fitted with an arbitrary function to obtain the quenching parameter for each ion (Michaelian and Menchaca-Rocha 1994, Boivin *et al* 2016). Therefore, the EDSE model could be more accurate. The models' quenching parameters were determined by fitting the light produced in a voxel as a function of LET. The models were compared quantitatively by comparing their depth-dose profiles and the 95% confidence intervals of the quenching parameters' fit.

2.4.1. Birks equation

The Birks model is given by the equation

$$\frac{dS}{dx} = \frac{ALET}{1 + kBLET} \quad (1)$$

where $\frac{dS}{dx}$ is the scintillation yield per unit length, A is the scintillation efficiency (emitted light per deposited energy), and kB is the quenching factor ($\mu\text{m keV}^{-1}$). The quenching factor is unique to the type of scintillator used and the type of incident particle. The Birks equation can be rewritten in terms of finite volume as

$$S_v = \frac{ALET_v}{1 + kBLET_v} \phi_v \quad (2)$$

where S_v is the light emitted in a volume v , LET_v is the track-averaged LET in that volume, and ϕ_v is the particle fluence in that volume.

2.4.2. EDSE equation

The EDSE model relates the ionization quenching to the deposition of energy by the secondary electrons along the track of the ion beam. The realization of the EDSE model is based on the difference in the spectrum of secondary electrons produced by ions of different atomic numbers. The electron energy deposition density as a function of radial distance r from the ion's track is given as (Michaelian and Menchaca-Rocha 1994)

$$\rho(r) = N \frac{e^4}{nm_e} \frac{z^{*2}}{V^2} \frac{1}{r^2} \left[1 - \frac{r}{R_{\max}} \right]^{d+\frac{1}{n}} \quad (3)$$

where m_e is the electron mass, N is the number of electrons per unit volume, z^{*2} is the effective charge of the ion, and V is the ion velocity. R_{\max} is the maximum range of the secondary electron, $n = 5/3$ is the exponent in the electron range-energy relation (Kanaya and Okayama 1972), and $d = 0.045 Z_{\text{eff}}$, where Z_{eff} is the effective atomic number of the medium. This equation is valid from the minimum impact parameter b_{\min} to R_{\max} (Michaelian and Menchaca-Rocha 1994). For example, the values of b_{\min} and R_{\max} for a 10 MeV proton are 1.5 nm and 10 μm , respectively. Integration over the radial distribution is equal to the specific energy loss, or LET for protons.

The energy carrier density per unit path length of the ion is

$$\frac{dN_e}{dx} = K \left[\pi r_q^2 \rho_q + \int_{r_q}^{R_{\max}} \rho(r) 2\pi r dr \right] \quad (4)$$

where ρ_q is the quenching parameter that is specific to the scintillator detector, and r_q is the corresponding quenching radius for a given value of ρ_q . The value K relates the energy deposited to the number of energy carriers formed. Finally, the scintillation yield per unit length is $\frac{dS}{dx} = A \frac{dN_e}{dx}$, where the value A is the scintillation efficiency. The integral in equation 4 can be solved analytically if the power in equation 3 is a rational number. For plastic scintillators with $Z_{\text{eff}} = 3.5$, this value can be approximated to $\frac{3}{4} (d + \frac{1}{n} = 0.76)$. Michaelian and colleagues (Michaelian *et al* 1995) have solved this integral analytically for common organic and inorganic scintillators.

Similarly to the Birks equation, we can rewrite this model in terms of a finite volume as

$$S_v = A N_{ev} \phi_v \quad (5)$$

where N_{ev} is the average value of energy carrier density in that volume.

2.5. Quenching correction factor

To determine the quenching correction factors per voxel, the quenching parameters for each model were determined using nonlinear least-square fitting of the measured scintillation light profile to the simulated scintillation light profile. The energy deposition in a voxel can be obtained by multiplying the track-averaged LET and particle fluence through that voxel as

$$E_v = LET_v \cdot \phi_v \quad (6)$$

Therefore, the quenching correction factor using the Birks equation is

$$QCF_v = \frac{1 + k B LET_v}{A} \quad (7)$$

Similarly, the EDSE model quenching correction factor per voxel can be determined by combining equations 5 and 6 thus

$$QCF_v = \frac{LET_v}{A N_{ev}} \quad (8)$$

3. Results

3.1. Optical corrections

Figure 3(a) shows the central Monte Carlo depth-dose distribution, depth-light distribution, and LET for a 100.9 MeV proton beam. The depth-light distribution was obtained from the projection in figure 3(b), including the optical corrections applied to it, which was called the original projection in methods section 2.3. The camera projection origin was set at the center of the scintillator for applications of optical

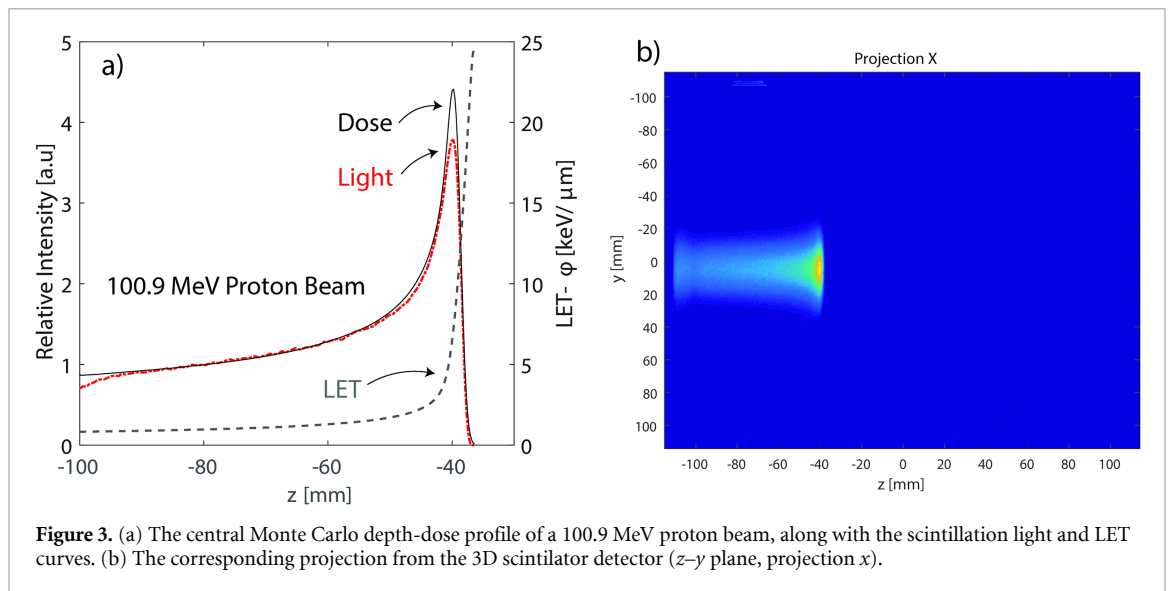


Figure 3. (a) The central Monte Carlo depth-dose profile of a 100.9 MeV proton beam, along with the scintillation light and LET curves. (b) The corresponding projection from the 3D scintillator detector (z - y plane, projection x).

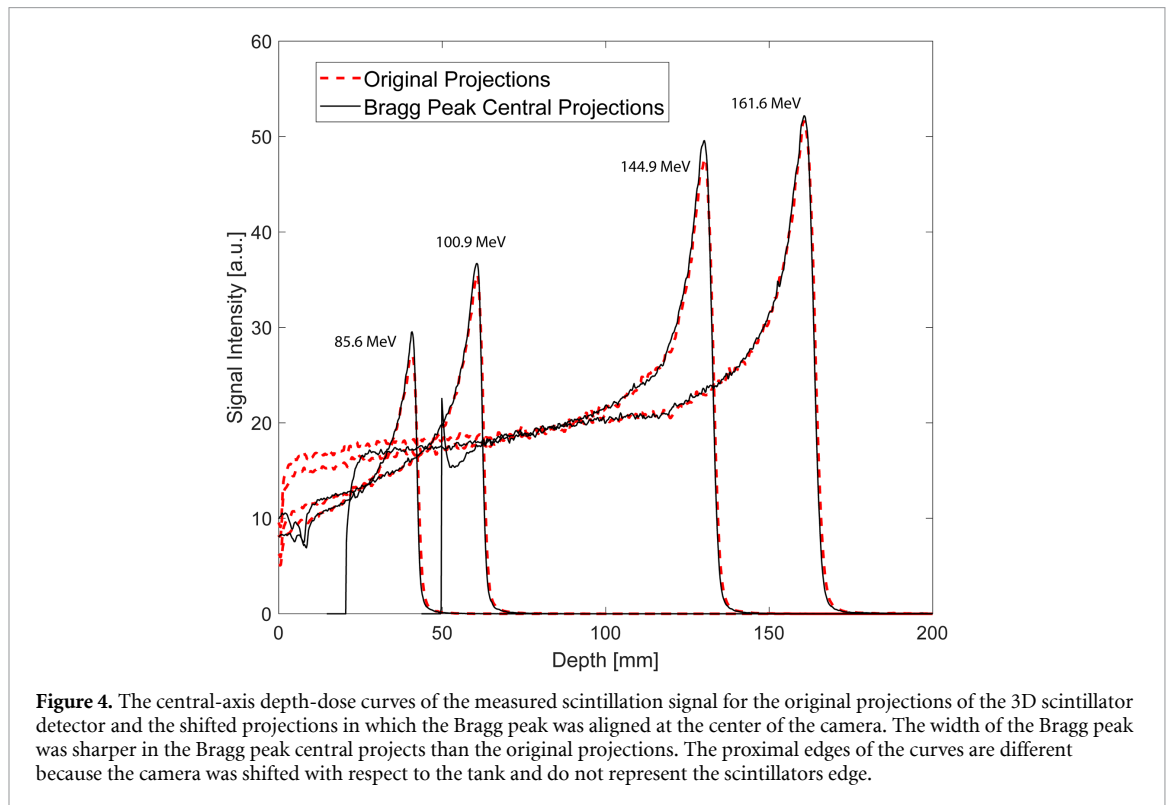


Figure 4. The central-axis depth-dose curves of the measured scintillation signal for the original projections of the 3D scintillator detector and the shifted projections in which the Bragg peak was aligned at the center of the camera. The width of the Bragg peak was sharper in the Bragg peak central projects than the original projections. The proximal edges of the curves are different because the camera was shifted with respect to the tank and do not represent the scintillators edge.

artifact corrections. The results for the Bragg peak central projections compared to the original projections for all four proton beams are shown in figure 4. Due to parallax error, the Bragg peak scintillation signals were higher for the Bragg peak central projections and varied as a function of beam energy (by 1%–8%). Furthermore, the Bragg peaks of the original projections were wider than those of the Bragg peak central projections by 2.87 ± 1.7 mm. Figure 4 shows different proximal edge signals for the Bragg peak central curves because the camera is shifted with respect of the scintillator. The true edges of the scintillator are determined by calibration marks placed on throughout the corners of the tank (Darne *et al* 2017).

3.2. Quenching model fitting

The quenching parameters for each model were determined by fitting the scintillation light to the MC dose and LET of each beam energy. Only points up to the distal 80% of the Bragg peak were included in the fitting. The reason for this cutoff was to minimize the uncertainty caused by the low level of scintillation light and the Monte Carlo dose and LET alignment. The major error was found around the Bragg peak and its distal edge. Figure 5 shows the effect of optics on the assignment of LET values for each voxel. The Bragg peak central projections (shown as unfilled markers) did not diverge as much as the original projections

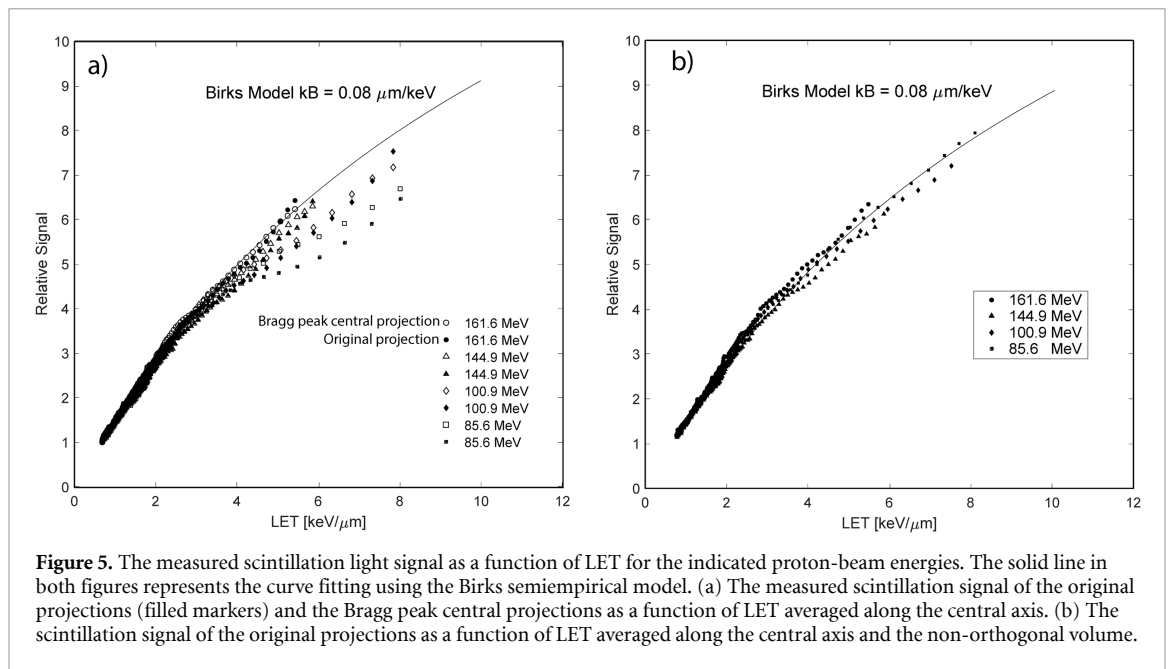


Figure 5. The measured scintillation light signal as a function of LET for the indicated proton-beam energies. The solid line in both figures represents the curve fitting using the Birks semiempirical model. (a) The measured scintillation signal of the original projections (filled markers) and the Bragg peak central projections as a function of LET averaged along the central axis. (b) The scintillation signal of the original projections as a function of LET averaged along the central axis and the non-orthogonal volume.

from the theoretical model fitting (solid line). This suggests the parallax error was reduced but not completely eliminated.

The best fit was obtained by comparing the scintillation light to a simulated projection (i.e. averaging the LET and dose along the nonorthogonal projections) as shown in figure 5(b), thereby confirming that the average LET value in a volume can be used to explain the scintillation response.

The measured k_B parameter was $0.083 \pm 0.003 \mu\text{m keV}^{-1}$ (95% confidence interval) with a normalization factor $A = 209 \text{ signal intensity/Gy}$. The quenching parameter for the EDSE model was $\rho_q = 23.4 \pm 5.7 \text{ keV } \mu\text{m}^{-3}$ (95% confidence interval) with a normalization factor of $A = 341 \text{ signal intensity/Gy}$. The EDSE parameter fit error was 24% and Birks was 3.61%. The higher error in the EDSE model parameter fit could be caused by some model simplifications in the determination of the electron radial distribution (Michaelian and Menchaca-Rocha 1994). The normalization factor A , differs from the scintillation efficiency factor mentioned above in that it accounts for the detector collection efficiency (i.e. it is a relative light yield measurement).

3.3. Quenching correction factors

Figure 6(a) plots the depth-dose curves at the central axis for the four beam energies tested in this study. The quenching correction factors were applied to correct the scintillation signal. Both quenching models are shown. The ratio of the dose as determined by Monte Carlo to the corrected dose using both models is plotted in figure 6(b). The average percentage difference between Monte Carlo and Birks model were within a range of $\pm 3\%$. While the average percentage difference between Monte Carlo and EDSE model were within a range of $\pm 7\%$. The dose difference at the Bragg peak was within $\pm 3\%$ for the Birks model and $\pm 6\%$ for the EDSE model. Table 1 shows the percent dose differences between the Monte Carlo and corrected and uncorrected scintillation signals at the Bragg peak for each proton beam energy.

4. Discussion

The major source of error in our study was the assignment of LET values for each voxel in the projection. The simulated projection showed that an average LET value can still be used to correct for quenching (as demonstrated in figure 5). Unfortunately, acquired projections cannot be corrected for parallax errors because the projection has already integrated the light distribution. The speed of volumetric scintillator detectors (all 94 beam energies can be measured in a few minutes) makes it feasible to use all 94 proton-beam energies to generate a calibration ‘look-up table’ of quenching correction factors based on the ratio of the scintillation response to dose. This will require further testing the stability and reproducibility of the light measurements and the calibration factors. For proton range verification, the detector has been shown to be reproducible and to have submillimeter accuracy for all 94 beam energies (Darne *et al* 2017).

The Birks equation compared to the EDSE model used in this study provided more accurate reproduction of the depth-dose curve. The accuracy of the EDSE model was limited by its approximations of the general expression of the electron energy deposition density per unit path length of the incident ion as a

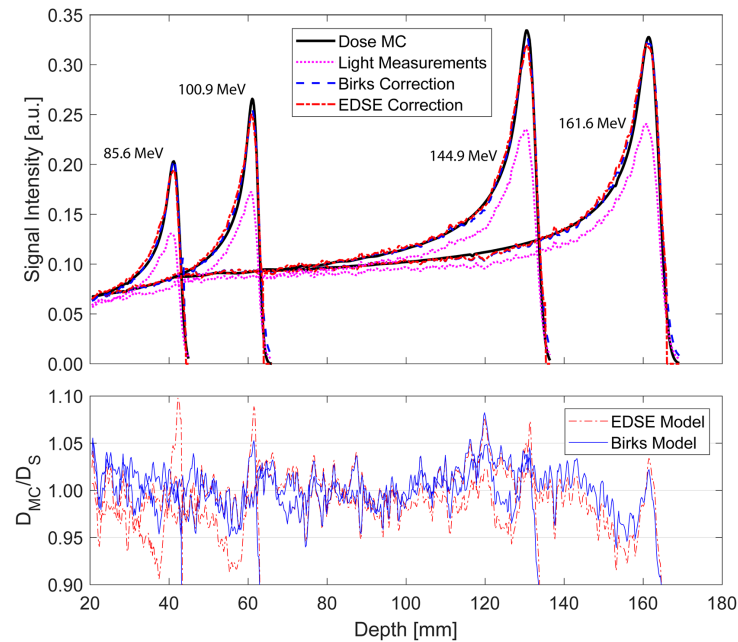


Figure 6. (a) The depth-dose profiles at the central axis for each proton-beam energy. The dose calculated using monte carlo (mc) simulation is compared to the corrected and uncorrected scintillation signals using the birks and edse models. (b) The ratio of the MC dose (D_{MC}) to corrected dose of the scintillator (D_s) for both models tested in this study.

Table 1. The percent difference from Monte Carlo of the Bragg peak height for each beam energy using the Birks and EDSE quenching correction factors.

Energy [MeV]	Bragg peak percent difference from Monte Carlo		
	Uncorrected	Birks Corrected	EDSE Corrected
161.6	40.44	0.17	0.86
144.9	42.57	3.00	4.87
100.9	56.75	2.60	5.25
85.6	57.92	0.43	3.85

function of radial distance. In this study, the Monte Carlo LET values were used to account for the energy spectrum in the EDSE model. It was achieved by normalizing the EDSE quenching correction factors by multiplying by LET, as shown in equation 8. This resulted in similar errors seen in figure 6(b). Although the EDSE model was less accurate than the Birks model in this study for 2D projection measurements, the EDSE model or similar models that are based on track structure provide a better understanding of ionization quenching for high LET values ($>12 \text{ keV } \mu\text{m}^{-1}$), for example in carbon ion beams, or in higher dose rates (Christensen *et al* 2019).

The proton beam used in this study and in a previous study by Robertson *et al* (2013) was from a synchrotron-based proton-beam accelerator, while the proton beam used by Almurayshid *et al* (2017) was produced using a fixed-proton-beam cyclotron. The phase space of a proton beam generated by a fixed-beam cyclotron does not change as a function of beam energy. Instead, an energy degrader is used to change the energy (or range) of the beam. In contrast, a synchrotron accelerates protons to each specified energy. Therefore, the phase space of the beam is energy dependent.

Optical parallax error affected the lower beam energies more than the higher beam energies produced by the proton-beam system. For low beam energies, the optical parallax error was exacerbated because the Bragg peak width for low beam energies is sharper than for higher energies. In the future, 3D reconstruction of the light distribution using maximum likelihood expectation maximization should improve the assignment of LET per voxel, which will improve the accuracy of quenching measurements in volumetric scintillators (Hui *et al* 2014).

5. Conclusion

In this study, quenching corrections using the Birks' and EDSE models were demonstrated for volumetric scintillator detectors. The Birks equation, which relies on the average LET value in a voxel, provided the best

fit for reproducing the measured proton depth-dose curves from a 3D scintillator. The usefulness of the EDSE model will be in accounting for quenching of different heavier ion beams. Camera parallax errors were the major source of uncertainty for sharp Bragg peaks and steep LET curves, which is caused by limited detector size. The nonorthogonal projections captured by an objective lens made quenching correction complicated for projection images. We have improved the application of Birks' model quenching corrections in 3D scintillators by numerically projecting the dose and LET 3D grid to camera projections. In our future work, we will obtain the light distribution in 3D from the three camera projections to simplify the application of quenching correction models in 3D scintillator detectors.

Acknowledgments

This work was supported by the National Cancer Institute of the National Institutes of Health (Award Number R01CA182450). The content is solely the responsibility of the authors and does not necessarily represent the official views of the National Institutes of Health. We would like to acknowledge Jeppe Brage Christensen for his discussions on ionization quenching models. The authors thank Dr. Narayan Sahoo for providing beam time support at the Proton Therapy Center and Dr. Dragan Mirkovic for providing Monte Carlo simulations support. We also thank Amy Ninetto from Scientific Publications, Research Medical Library at The University of Texas MD Anderson Cancer Center for editing our manuscript.

Conflicts of interest

The authors have no conflicts of interest to disclose.

Funding

This work was supported by the National Cancer Institute of the National Institutes of Health (Award Number R01CA182450). The content is solely the responsibility of the authors and does not necessarily represent the official views of the National Institutes of Health.

ORCID iDs

Fahed Alsanea  <https://orcid.org/0000-0001-5491-6565>

Sam Beddar  <https://orcid.org/0000-0001-5825-110X>

References

- Almurayshid M, Helo Y, Kacperek A, Griffiths J, Hebden J and Gibson A 2017 Quality assurance in proton beam therapy using a plastic scintillator and a commercially available digital camera *J. Appl. Clin. Med. Phys.* **18** 210–19
- Alsanea F, Darne C, Hojo Y and Beddar S 2019 A novel imaging scheme for optical cameras used in a quality assurance detector for discrete spot scanning proton beam systems *Nucl. Instrum. Methods Phys. Res. Sect.* **939** 16–21
- Archambault L, Poenisch F, Sahoo N, Robertson D, Lee A, Gillin M T, Mohan R and Beddar S 2012 Verification of proton range, position, and intensity in IMPT with a 3D liquid scintillator detector system *Med. Phys.* **39** 1239–46
- Beddar S, Archambault L, Sahoo N, Poenisch F, Chen G T, Gillin M T and Mohan R 2009 Exploration of the potential of liquid scintillators for real-time 3D dosimetry of intensity modulated proton beams *Med. Phys.* **36** 1736–43
- Birks J B 1964 *The Theory and Practice of Scintillation Counting: international Series of Monographs in Electronics and Instrumentation* (Oxford: Pergamon Press)
- Blanc D, Cambou F and Lafond Y G D 1964 Étude cinétique de la scintillation dans les cristaux organiques purs *J. Phys. France* **25** 319–25
- Boivin J, Beddar S, Bonde C, Schmidt D, Culbertson W, Guillemette M and Beaulieu L 2016 A systematic characterization of the low-energy photon response of plastic scintillation detectors *Phys. Med. Biol.* **61** 5569
- Bouquet J 2010 *Camera Calibration Toolbox for MATLAB* (Pasadena, CA: California Institute of Technology)
- Chou C N 1952 The nature of the saturation effect of fluorescent scintillators *Phys. Rev.* **87** 904–5
- Christensen J B, Almhagen E, Stolarczyk L, Vestergaard A, Bassler N and Andersen C E 2019 Ionization quenching in scintillators used for dosimetry of mixed particle fields *Phys. Med. Biol.* **64** 095018
- Christensen J B and Andersen C E 2018 Relating ionization quenching in organic plastic scintillators to basic material properties by modelling excitation density transport and amorphous track structure during proton irradiation *Phys. Med. Biol.* **63** 195010
- Darne C, Robertson D, Alsanea F and Beddar S 2016 SU-D-BRC-07: system design for a 3D volumetric scintillation detector using CMOS Cameras *Med. Phys.* **43** 3337–3337
- Darne C D, Alsanea F, Robertson D G, Sahoo N and Beddar S 2017 Performance characterization of a 3D liquid scintillation detector for discrete spot scanning proton beam systems *Phys. Med. Biol.* **62** 5652
- Fukushima Y, Hamada M, Nishio T and Maruyama K 2006 Development of an easy-to-handle range measurement tool using a plastic scintillator for proton beam therapy *Phys. Med. Biol.* **51** 5927
- Grün R, Friedrich T, Traneus E and Scholz M 2019 Is the dose-averaged LET a reliable predictor for the relative biological effectiveness? *Med. Phys.* **46** 1064–74

- Hui C, Robertson D and Beddar S 2014 3D reconstruction of scintillation light emission from proton pencil beams using limited viewing angles—a simulation study *Phys. Med. Biol.* **59** 4477
- Hui C K, Robertson D, Alsanea F and Beddar S 2015 Fast range measurement of spot scanning proton beams using a volumetric liquid scintillator detector *Biomed. Phys. Eng. Express* **1** 025204
- Kanaya K and Okayama S 1972 Penetration and energy-loss theory of electrons in solid targets *J. Phys. Appl. Phys.* **5** 43
- Michaelian K and Menchaca-Rocha A 1994 Model of ion-induced luminescence based on energy deposition by secondary electrons *Phys. Rev. B* **49** 15550–62
- Michaelian K, Menchaca-Rocha A and Belmont-Moreno E 1995 Scintillation response of nuclear particle detectors *Nucl. Instrum. Methods Phys. Res. Sect.* **356** 297–303
- Pönisch F, Archambault L, Briere T M, Sahoo N, Mohan R, Beddar S and Gillin M T 2009 Liquid scintillator for 2D dosimetry for high-energy photon beams *Med. Phys.* **36** 1478–85
- Robertson D, Hui C, Archambault L, Mohan R and Beddar S 2014 Optical artefact characterization and correction in volumetric scintillation dosimetry *Phys. Med. Biol.* **59** 23–42
- Robertson D, Mirkovic D, Sahoo N and Beddar S 2013 Quenching correction for volumetric scintillation dosimetry of proton beams *Phys. Med. Biol.* **58** 261
- Sawakuchi G O, Mirkovic D, Perles L A, Sahoo N, Zhu X R, Ciangaru G, Suzuki K, Gillin M T, Mohan R and Titt U 2010 An MCNPX Monte Carlo model of a discrete spot scanning proton beam therapy nozzle *Med. Phys.* **37** 4960–70
- Wang L L W, Perles L A, Archambault L, Sahoo N, Mirkovic D and Beddar S 2012 Determination of the quenching correction factors for plastic scintillation detectors in therapeutic high-energy proton beams *Phys. Med. Biol.* **57** 7767–81
- Waters L S, Hendricks J and McKinney G 2002 *Monte Carlo N-particle Transport Code System for Multiparticle and High Energy Applications* (Los Alamos, NM: Los Alamos National Laboratory)